Available online at www.sciencedirect.com
SCIENCE DIRECT®
Continental Shelf Research 25 (2005) 1473–1497
CONTINENTAL SHELF RESEARCH
www.elsevier.com/locate/csr

On the fluctuations and vertical structure of the shelf circulation off Walvis Bay, Namibia

Hans Ulrich Lass*, Volker Mohrholz

Institut für Ostseeforschung Warnemünde, Seestrasse 15, D-18119 Rostock-Warnemünde, Germany

Received 4 August 2004; received in revised form 3 March 2005; accepted 25 April 2005
Available online 29 June 2005

Abstract

Temporal variations of the current field on the shelf of the South East Atlantic off Walvis Bay were studied during austral summer and fall by moored current profiler and temperature-salinity recorder located on the shelf 20 nm off Walvis Bay, Namibia. Spatial and temporal variations of the wind field in the South East Atlantic were investigated by 3-day averaged wind fields measured by the QuikSCAT satellite. The local wind was provided by a time series of hourly wind vectors measured on a moored buoy off Swakopmund.

The significant tidal motion on the shelf off Walvis Bay is composed of the anticlockwise rotating barotropic semidiurnal constituents M2 and S2. The tidal currents are described to a first order by a barotropic deep ocean Kelvin wave.

The land-sea breeze forces anticlockwise rotating diurnal variations of the current in the surface mixed layer and an opposite directed current below the thermocline, which compensates the mass flux normal to the coast in the surface layer.

Most of the energy of the current fluctuations were concentrated around the local inertial period of $T_i = 30.7$ h. These fluctuations consisted of at least four significant anti-clockwise rotating vertical modes with amplitudes ranging between 10 and 20 cm/s. On a large scale the amplitudes of inertial motions correlate with the wind fluctuations but locally the motions consist of a superposition of locally wind forced inertial oscillations and inertial waves generated at larger distances as well near the surface as close to the bottom. The vertical structure of the inertial motion suggests that it could be a possible candidate for mixing in the bottom boundary layer by differential advection.

Coastal trapped waves of horizontal mode number less that four were observed at periods of about 7 days.

The mean cross shelf circulation consisted of a two cell structure. The upper cell was made of the Ekman offshore current and a compensating onshore current at intermediate depth below the thermocline. The lower cell consisted of an offshore current in the bottom layer below 80 m depth and was closed by the onshore current in the intermediate depth range. The cross shelf circulation controlled the fraction of ESACW on the shelf water mass.

The long shelf circulation consisted in the surface mixed layer of an equatorward coastal jet driven by the local meridional wind stress and an almost barotropic poleward counter current appearing partly as free Kelvin wave emanating from the Angola-Benguela front and as coastal counter current forced by the local negative curl of the wind

*Corresponding author. Tel.: +49 3815197130.
E-mail address: lass@io-warnemuende.de (H.U. Lass).

0278-4343/$ - see front matter
doi:10.1016/j.csr.2005.04.012

stress. The longshore current controlled the fraction of the SACW on the shelf water mass, which increased continuously between austral summer and fall.

Keywords: Shelf dynamics; Semidiurnal tides; Inertial waves; Shelf waves; Water circulation; Wind-driven currents; Benguela current

1. Introduction

The Benguela, as one of the four major eastern boundary current regions of the World Ocean, is a broad northward flow off southwestern Africa and is part of the South Atlantic subtropical gyre. It is driven by the large-scale wind patterns and thermohaline forcing (Garzoli and Gordon, 1996). The currents on the shelf off Namibia and South Africa are known as the Benguela upwelling system, which is forced locally by the wind stress field in the South East Atlantic (Nelson and Hutchings, 1983). General descriptions of the Benguela upwelling system are given by Shannon (1985) and Shannon and Nelson (1996).

The Benguela upwelling system stretches from the southern tip of Africa to the Angola-Benguela front located at about 15–16°S, which separates the warm water of the Angola Current from the cold Benguela water. The area of the Benguela is exposed to a persistent alongshore wind associated with the St. Helena high pressure system. The upwelling favourable alongshore wind has a maximum at about 25°S and decreases toward the northern and southern boundaries of the Benguela system at the Angola-Benguela front and the southern tip of Africa, respectively. In the south the winds are highly seasonal and reach maximum during austral spring and summer (Boyd, 1987; Shannon and Nelson, 1996). North of 31°S the seasonal variation is weaker with permanent alongshore winds with a spring–summer maximum and autumn minimum as far north as 25°S. North of that latitude the maximum occurs in late winter to spring and a minimum occurs in summer–autumn. The alongshore wind stress increases away from the coast resulting in a band of cyclonic wind stress curl along the coast which confluences with a cyclonic wind stress curl in the area of the Angola Gyre as shown by Bakun and Nelson (1991).

An important branch of the circulation in the Benguela upwelling system is the poleward undercurrent which stretches from the northern Benguela (Hagen, 1991), toward the Cape Basin in the south (Nelson, 1989), partly at the shelf edge and partly on the shelf. The poleward current extends to the surface in the area of the Angola-Benguela front (Lass et al., 2000). Yamagata and Iizuka (1995) found some indications that coastal Kelvin waves, which originate from north of the Angola-Benguela front, export the poleward current south of the front where it may superimpose with the wind-driven equatorward surface current (Gründlingh, 1999). Fennel (1999) has shown that the wind stress curl off Namibia produces a secondary divergence of the Ekmann offshore transport and forces upwelling and a downwind surface flow offshore and a poleward countercurrent in the coastal strip of weak meridional wind stress. Temporal variations of the poleward current in the northern Benguela comprises multiple time scales reaching from seasons to a few days while its variations in the southern Benguela become weaker at longer time scales (Shannon and Nelson, 1996). Continental shelf waves are thought to determine the current fluctuation in the Benguela upwelling system with periods of several days (Hagen, 1979; Nelson, 1989; Gründlingh, 1999).

One of the major features in the South East Atlantic is the occurrence of large areas throughout which very low oxygen concentrations are found (see Chapman and Shannon, 1985 for a review). This area covers the thermocline waters of the Angola gyre and extends from the southern rim of the gyre wedge like along the shelf of the Benguela region as far south as 25°S but sometimes up to the Orange River (29°S). The oxygen

depleted water on the Namibian shelf has two separate cores, one located at the shelf break in about 300 m depth and one in the bottom layer of the upper shelf in the depth range between 150 and 50 m on top of the diatomic mud belt. Hart and Currie (1960) suggested and Stander (1964) provided further evidence that the water with low oxygen concentration at the shelf break is advected by the poleward undercurrent from the area of the Angola Gyre. Chapman and Shannon (1987) stressed that the oxygen depleted water on the shelf off Walvis Bay is maintained by the decomposition of sinking organic matter exported northward from the Lüderitz upwelling cell. Variations of the upwelling intensity in the Lüderitz cell with time scales ranging from season to a weak combined with similar changes in the ventilation of the sub-thermocline water may imply the occurrence of anoxic water and the occasional appearance of hydrogen sulphide on the shelf in the area off Walvis Bay (Copenhagen, 1953; Hart and Currie, 1960; Stander, 1964). Weeks et al. (2004) have shown that sulphide eruptions are by far more widespread in space and time than hitherto known with devastating consequences on the upper trophic levels of the Benguela ecosystem. An improved knowledge on the advection and mixing of water masses at the shelf off Walvis Bay is prerequisite for a better understanding of the reasons and of the spatial and temporal patterns of sulphide eruptions. The ventilation of the water on the shelf processes is controlled by both the local forced and the remote forced dynamical processes. While the remotely forced poleward undercurrent buffers the formation of hydrogen sulphide by transporting oxygen depleted but nutrient enriched water from the Angola Gyre along the shelf of the Benguela, the locally forced cross shelf circulation, carries well ventilated ocean water onto the shelf. Hence, both might be important for the distribution and triggering of anoxia and hydrogen sulphide eruptions.

Current profile observations performed on the shelf off Walvis Bay, Namibia, during austral summer were analysed with respect to their vertical structure at various time scales. The aims of these studies were to understand how the different dynamical processes involved contribute to the ventilation and mixing of the subthermocline water on the shelf off Walvis Bay and how they are controlled by local and remote wind fields.

2. Data and methods

Hydrogen sulphide eruptions are a common phenomenon at the coast off Walvis Bay in particular during austral summer. The selected time and site, located 20 nm off Walvis Bay in the area of the diatomic mud belt in a water depth of about 130 m, appeared suitable to study the ventilation of the shelf water by currents with respect to sulphide eruptions.

In order to put the observations at a single mooring in a larger perspective, satellite observations would be a suitable method in order to associate spatial scales of the current field with the temporal variations of the currents revealed by the ADCP. The standard deviations of sea surface topography measurements by TOPEX/POSEIDON and ERS2 are 2 and 3 cm, respectively. The error of a single sea level elevation measurement on the shelf may be even larger due to uncertainties of the tidal correction on the shelf (Greiner and Arnault, 2000). Given a typical standard deviation of 6 cm for the de-tided sea level at Walvis Bay present satellite topography seems to be too inaccurate to give a reliable estimate of the sea surface topography on the shelf of an eastern boundary current system with time scales less than 10 days.

Deformation of thermal gradients seen by satellite sea surface temperature measurements have been used by Gründlingh (1999) to study spatial inhomogeneous near surface current fields. Significant thermal gradients are located at the shelf edge and at the shelf slope. Both are too distant from the position of the moored current meter data at hand. An alternative approach to combine temporal and spatial scales of the current field would be the comparison of moored current meter data with corresponding data of realistically forced model simulations. This work is in progress but would go beyond the scope of this paper.

2.1. Wind and tide gauge data

Wind data were downloaded for the period from 1 November 2002 to 14 April 2003 from Remote Sensing Systems (http://www.remss.com/) ftp directories containing global distributed wind vectors as bytemaps. Each file associated to 1 day consists of wind of data averaged over the last 3 days. The data are gridded into 0.25° lat/lon cells. The wind vectors were extracted from the files for selected areas off Walvis Bay, which are representative for the local wind forcing, the equatorial belt of the Atlantic, and along a route from the Gulf of Guinea to the core of the subtropical anticyclone in the South Atlantic with the full spatial resolution. The latter two are important areas for the remote forcing of currents off Namibia. Wind stress was computed from the daily QuikSCAT data according to Fairall et al. (1996) using the MATLAB Air-Sea toolbox version 2.0 (http://seamat.whoi.edu/). The comparison of wind vectors measured by QuikSCAT and measured on research vessels revealed a RMS difference of 16° with respect to direction (http://www.coaps.fsu.edu/~bourassa/QSCAT_CV/all_egg_d.html) and 1.2 m/s with respect to wind speed (http://www.coaps.fsu.edu/~bourassa/QSCAT_CV/all_egg_s.html).

Additionally, two time series of hourly wind vectors, one measured on board of the meteorological buoy located 5 km offshore from Swakopmund, Namibia, the other measured at the shore of Swakopmund (NatMIRC building) were made available by the National Marine Information and Research Centre in Swakopmund. These wind date compared well with each other except for periods less than 10 h. The wind spectrum measured at the buoy was noisier than the shore station data in this high frequency range.

Tide gauge data measured with a sampling time of 10 min in the harbour of Walvis Bay, Namibia, were provided by NatMIRC too.

2.2. Mooring

In order to obtain information on the temporal variability of hydrographic parameters on the central Namibian shelf an oceanographic mooring was deployed at the hydrographic transect in 20 nm distance to the coast (Station 020 in Fig. 1) at about 130 m water depth. The mooring was equipped with an upward looking 300 kHz Workhorse ADCP, four Seacat SBE 16 recorders and three Seamon temperature recorders with the specifications given in Table 1 and shown in Fig. 2. The mooring was deployed at 9 December 2002, recovered at 11 February 2003 and redeployed a few hours later at the same position. The final recovery of the mooring took place at 1 April 2003. The data recovery rate was 100%.

2.3. ADCP

The 300 kHz RDI Workhorse ADCP was mounted upward looking in the mooring line such that the sound rays, directed 20° off the instrument axis, did not interfere with any part of the mooring. The estimated transducer depth was 121 m. The bin size was 4 m. A burst of 150 pings was vector averaged every hour and stored together with backscattering intensity, correlation and percent good in the internal memory. The resulting standard deviation of the ensemble averaged velocities at a distance within 120 m from the transmitter is about 0.2 cm/s. A compass calibration was performed just before the deployment of the mooring while the local magnetic variation of 17° toward west was corrected after recovering the data. The upper bins, affected by side lobe effects, were removed from the record resulting in an uppermost reliable depth level of 14 m.

The tilt of the ADCP was always less than $\pm 6^\circ$ during the deployment, indicating that the mooring was quite stable. The moored ADCP was subject to rotations with the inertial period as indicated by the recorded heading measurements of the ADCP. The ADCP data were validated in two steps. First, values were discarded where the absolute of error velocity or vertical velocity exceeded 5 cm/s, or the mean backscattering was less than 40 counts, or the correlation was less than 80 counts. Missing values were replaced by two-dimensional interpolation. Second, the time series of horizontal velocity components of every depth

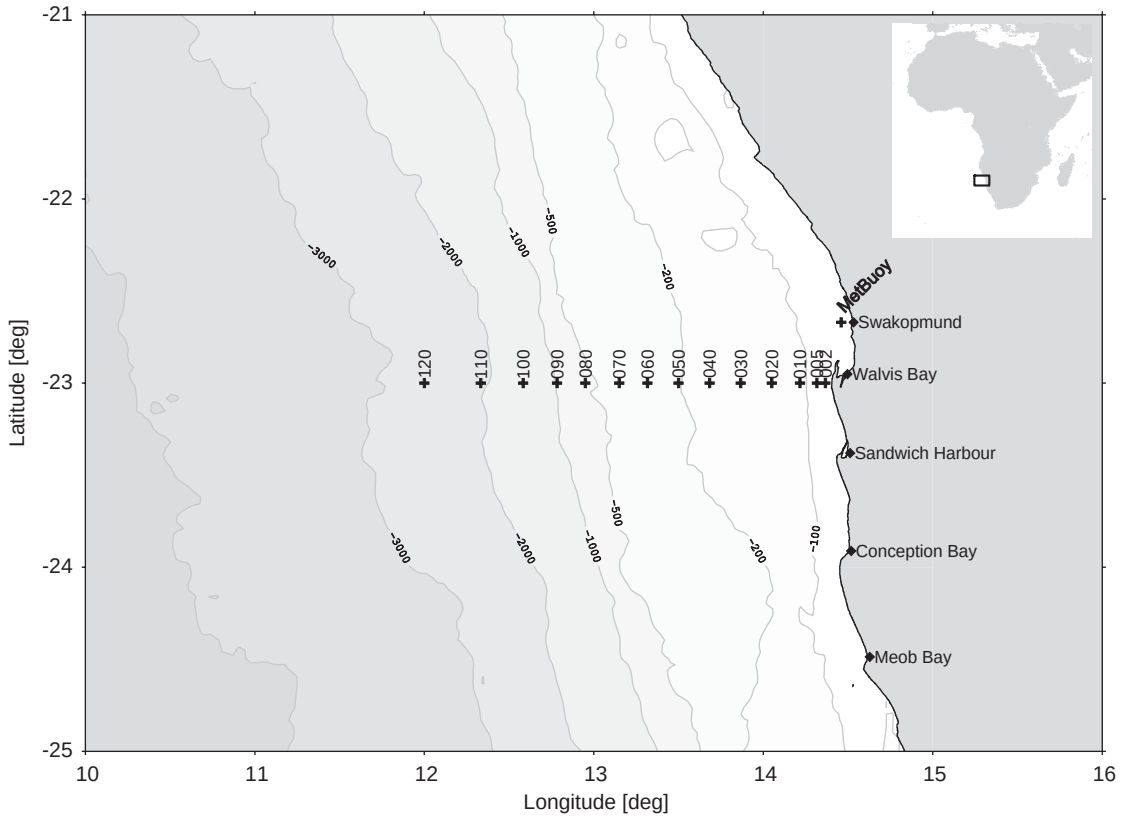

Fig. 1. Location of the hydrographic section covered during M57/2-3 roughly weekly between 12 February and 1 April 2003. The mooring M2002_15 was located 1 nm north of station 020. The meteorological buoy off Swakopmund is denoted as MetBuoy.

Table 1
Depths, sampling times and sensors of the moored instruments deployed from 9 December 2002 to 1 April 2003

Instrument	Sensors	Sampling time (min)	Depth (m)
Seamon	T	10	14
Seacat	T,S	60	24
Seamon	T	10	44
Seacat	T, S, O2(SBE 23)	60	65
Seamon	T	10	79
Seacat	T, S, O2(SBE 43)	60	95
WH ADCP	U,v,w,backscatter	60 (burst of 15 pings)	121
Seacat	T, S, O2(SBE 43)	60	125

bin was analysed for outliers by a median filter technique. Outliers were replaced by the median value taken over 11 time steps.

2.4. Seacats

The four Seacat SBE 16 recorders equipped with anti-fouling cells by the manufacturer and three SeaMon temperature recorders were calibrated prior and after the deployment in the calibration laboratory of the IOW. There was no shift in the temperature calibration and only minor differences for calibration coefficients of salinity sensors prior and after the deployment. Biological fouling may affect the accuracy of conductivity measurements by Seacat recorders in high productive areas by several 0.01 PSU even if they are equipped with anti-fouling cells. Therefore, intercalibration measurements by a ship based SBE911+CTD were carried out in the frame of the R/V Meteor cruises M57/2 and M57/3 from 11 February to 1 April once a week at station 020 which was at a distance

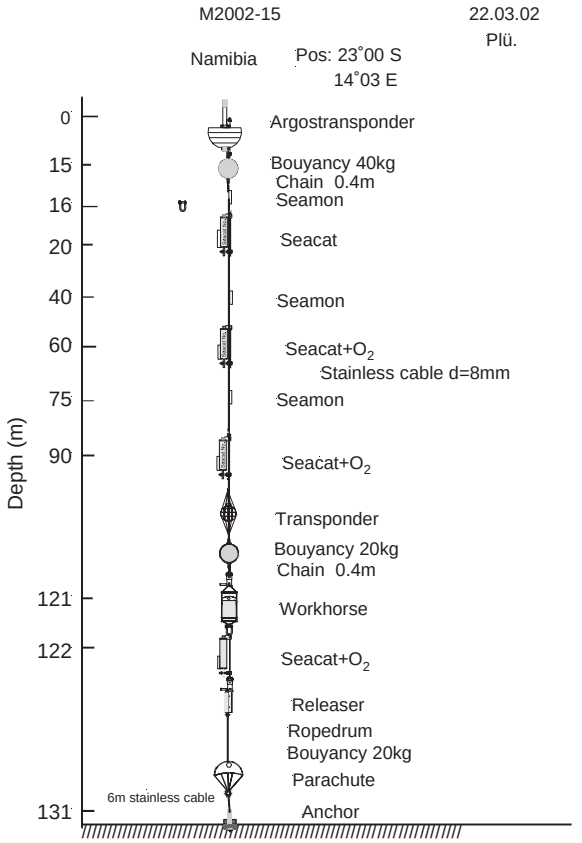

Fig. 2. Subsurface mooring equipped with an upward looking WH ADCP at 121 m nominal depth and 4 Seacat TS recorder. The Seacats in 60, 90 and 122 m nominal depth were equipped with SBE oxygen sensors. Auxiliary equipment consisted of an ARGOS watchdog, an acoustic transponder and an acoustic releaser. The actual depths of the instruments are somewhat different due to sinking of the anchor into the muddy sediment and real lengths of the mooring ropes, see Table 1.

of about 1 km from the mooring. These measurements were used to monitor the accuracy of the moored sensors. From differences in the temperatures between CTD and the moored temperature recorders the actual mounting depth of each moored instrument was corrected. These corrections were in agreement with the mean distance between the sea surface and the ADCP transducers measured by the ADCP itself. Constant shifts, shown by three of the salinity sensors compared to the CTD measurements, were corrected. After the validation the remaining rms error of the SeaMon temperature sensors amounts to 0.025 K. For the Seacat temperature and salinity measurements remaining rms errors of 0.005 K and 0.01PSU were estimated, respectively. The remaining error for the salinity measured by the Seacat mounted in 60 m depth was 0.02 PSU. Unfortunately, the SeaCat at 25 m depth was mounted in the centre of the thermocline. The very high vertical gradients in this layer caused a high sensitivity of this record to small vertical movements, due to internal waves and tilt changes of the mooring. Therefore, this instrument could not be corrected by intercomparison with the CTD measurements.

2.5. Complex empirical orthogonal function analysis

In order to study the vertical structure of current and temperature profiles the Complex Empirical Orthogonal Function (CEOF) analysis was employed, see Emery and Thomson (2001) for applications in oceanography. The cross spectra $S_{kl}(\omega)$ were calculated between every combination of measured depths k and l with about 10 effective degrees of freedom. Measured horizontal current vectors were transformed into complex numbers $u + i^*v$, where u is the zonal and v is the meridional current component, respectively. Eigenvalues and eigenvectors of the Hermitian matrices $S_{kl}(\omega)$ were estimated for every frequency band ω. The eigenvalues of a parameter represent the total variance of a mode while the corresponding eigenfunctions represent the vertical structure of this mode in a frequency band. Interfering different dynamical regimes can be analysed objectively by this method. However, the CEOF analysis provides no access to the amplitudes of a selected dynamical process in the time frame, which are needed to study the correlation of this process with e.g. a forcing parameter. In order to obtain the amplitudes of a process, e.g. the inertial motions, the time series measured in each depth were band pass filtered with a frequency range belonging to this process. Then these band pass filtered profiles were projected onto the vertical eigenfunctions at the peak of the spectrum of eigenvalues within the choosen frequency band

providing the amplitudes of the process in the time domain.

3. Results

3.1. Wind measurements

3.1.1. Walvis Bay

The wind stress off Walvis Bay was analysed between the longitude 10°E and the coast and the latitudes 25–21°S as a representative area for the local wind forcing. The northward component of the wind stress averaged within this latitudinal belt is shown as a longitude-time plot in Fig. 3. The meridional component of the wind stress appears as a sequence of temporal pulses with a time scale of about 1 week. Strong wind stress pulses occurred in November 2002 and in late March 2003. Weak pulses were observed in December 2002 and February 2003 while in January 2003 pulses appeared of moderate strength. The meridional wind stress was characterised by a cyclonic wind stress curl due to its increase from the coast toward the open ocean. This pattern of the wind stress supports aside of the coastal upwelling an upwelling at the maximum of the wind stress curl which is located in the average at about 13°E, the shelf edge off Walvis Bay.

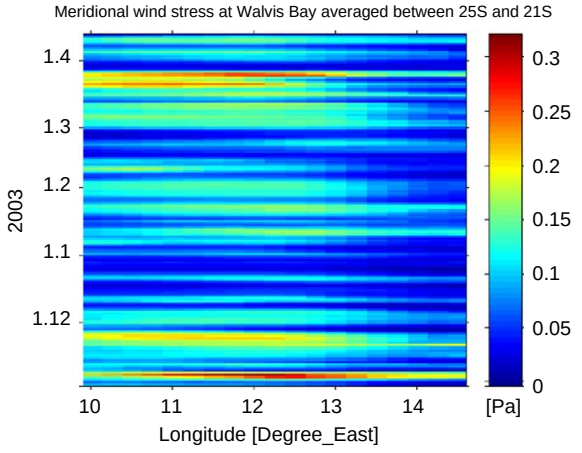

Fig. 3. Meridional component of the wind stress off Walvis Bay from 1 November 2002 to 10 April 2003 averaged within the latitudinal belt 25°S to 21°S.

3.1.2. Gulf of Guinea area

The wind stress in the Gulf of Guinea is weak in the northeastern corner while the SE trade winds strengthen toward southwest. This implicates an Ekman transport divergence along a line, which stretches from the Angola-Benguela front roughly towards northwest. In order to describe the temporal fluctuations of this divergence the wind stress component toward 295° from north was extracted along a line from the Gulf of Guinea toward the centre of the subtropical anticyclone in the South Atlantic, see Fig. 4. The corresponding wind stress component is generally weak in the Gulf of Guinea. An area of strong wind stress toward 295° was observed in the latitudinal belt located between 10°S and 25°S in the average. This wind stress component decreases once again south of about 25°W, the core area of the St. Helena anticyclone. The Ekman divergence, associated with the equatorward boundary of the intensified wind stress, implies open ocean upwelling and a cyclonic circulation with the South Equatorial Counter Current (SECC) north and the South Equatorial Current (SEC) south of this boundary. The SECC hits north of the Angola-Benguela front the African coast and contributes to the Angola Current. The Ekman divergence is exposed

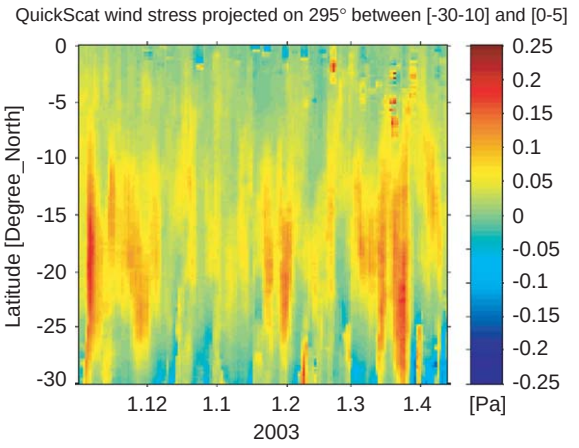

Fig. 4. Wind stress component toward 295° from north along a line from the Gulf of Guinea at 0°E and 5°E toward the centre of the subtropical anticyclone in the South Atlantic at 30°S and 10°W. The selected period of wind stress is from 1 November 2002 to 10 April 2003.

to temporal fluctuations with a time scale of about 8 days. The divergence was particular strong during November 2002, end of January 2003 and late March 2003.

3.1.3. Angola-Benguela front

The meridional wind stress in the area of the Angola-Benguela front averaged in the latitudinal belt between 20°S and 13°S is shown in Fig. 5. This wind stress component is strong in a belt between about 8°E and the coast in November 2002, becomes generally weak from December 2002 to March 2003 and increases after mid of March 2003 again. Pulses of relatively weak northward wind stress occur within this phase from December 2002 to March 2003 until mid of December 2002, at mid of January, and at the end of February to mid of March. The phases of strong meridional wind stress in the area of the Angola-Benguela front are correlated with the fluctuations of the curl of the wind stress in the area of the Angola gyre, see Fig. 4.

3.1.4. Off Swakopmund

The spectrum of the windvector measured at the meteorological buoy off Swakopmund, shown in Fig. 6, exhibits one broad peak distributed over the period range between 4 and 10 days, a narrow peak at the diurnal period and a second narrow peak at the semi-diurnal period. The power spectrum of the wind has the maximum energy density at the diurnal period. While the variations of the wind vector at the 10-day period are linearly polarised, an anticlockwise rotation dominates over the clockwise rotation at the diurnal period and the semi-diurnal period has a pure anti-clockwise rotation. The eccentricity of the rotating wind vectors is weak at both the diurnal and semi-diurnal period since the relation of the minor axis to the major axis is 0.8 and 0.9, respectively.

The diurnal peak in the wind spectrum oscillation is mainly due to the sea breeze effect which is well developed at the coast of Namibia, Shannon and Nelson (1996), while the semidiurnal peak is due to solar thermal semidiurnal tide which is associated with the well known semidiurnal surface pressure oscillations around the globe, Whiteman and Bian (1995).

3.2. Current measurements

The horizontal and vertical components of the current profiles were analysed by means of the Complex Empirical Orthogonal Functions as described in Section 2.5. The eigenvalues of the

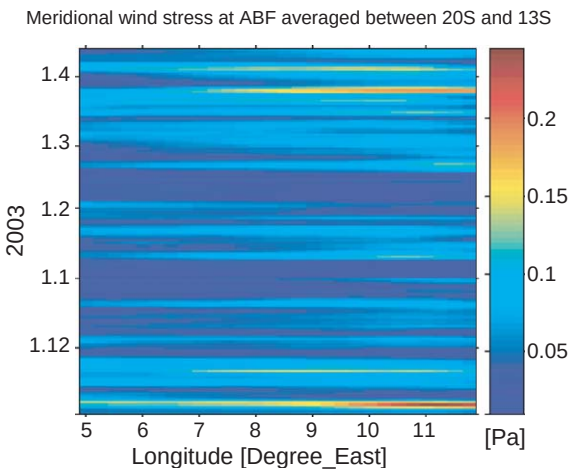

Fig. 5. Meridional component of the wind stress in the area of the Angola-Benguela front from 1 November 2002 to 10 April 2003 averaged within the latitudinal belt 20°S to 13°S.

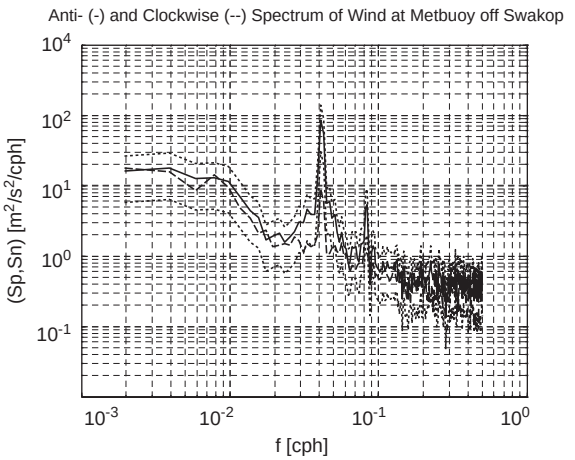

Fig. 6. Rotary spectra of the wind vector measured on the moored buoy off Swakopmund. The solid line represents the anti-clockwise and the dashed line the clockwise spectrum, respectively. The dotted lines are the confidence limits with 95% probability.

analysis of the horizontal current components are shown in Fig. 7 for clockwise rotating ($f<0$) and anti-clockwise rotating ($f>0$) currents. The major part of the energy of the current fluctuations is concentrated in four frequency bands of the anti-clockwise rotating currents. These bands are the semidiurnal tide band, the diurnal band, the band containing both the inertial oscillation and inertial waves at periods close to 30 h, and the Continental Shelf Wave band with a period of about 7 days. The clockwise rotating current fluctuations are generally weak but contain a band around the semidiurnal band and a band near the longest resolved period of about 20 days. The inertial band is the only one containing significant contributions of baroclinic modes. The duration of the current time series is too short to resolve the partial tidal components by power spectral analysis. Hence, a tidal analysis was done separately below.

3.2.1. Tidal analysis

The vertical structures of the first vertical eigenfunction at both the clockwise and anticlockwise semidiurnal tide band are shown in the lower panel of Fig. 8. The eigenfunction of the anti-clockwise rotating semi diurnal tide reveals a classical barotropic mode structure while the clockwise rotating component of the semidiurnal tide depicts a slight deviation of the pure barotropic structure in the upper half of the water column. The first vertical eigenfunction of the diurnal tide band depicts a baroclinic structure, see lower right panel of Fig. 9. This indicates that the motion in the diurnal tide band could be either a baroclinic tide or might be a motion forced by the diurnal land-sea breeze which provides a pronounced variability of the wind field near the coast of SW Africa, see Shannon and Nelson (1996) for a review.

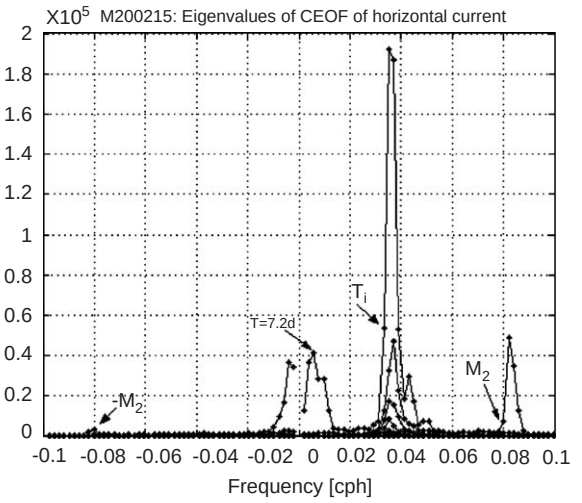

Fig. 7. Eigenvalues of the Complex Empirical Orthogonal Function analysis of the horizontal current off Walvis Bay. Positive frequencies mean anti-clockwise rotating current vectors and negative frequencies mean clockwise rotating current.

The tidal analysis toolbox according to Pawlowicz et al. (2002) was employed which uses harmonic analysis to estimate tidal constituents and their uncertainties in scalar and vector time series. The tidal analysis was performed for the tide gauge record at Walvis Bay harbour for the period from 09 January 2003 to 23 May 2003 and for the vertical averaged current at the mooring site from 10 December 2002 to 1 April 2003. The results are given in Table 2. Four significant tidal constituents were found in both the sea level elevation and the current measurements, the K1 of the diurnal tide and the N2, M2, and S2 of the semidiurnal tidal band. The signal to noise ratio of tidal amplitudes of the sea level elevations was generally better than those of the current measurements. The semidiurnal tide is the dominating one at Walvis Bay where the sum of diurnal constituents K1 and O1 is about 3% of the sum of the semidiurnal constituents M2 and S2. The major axis of the tidal ellipse of the current is aligned north–south; that means parallel to the local topography. Assuming that the tidal motion is determined by a perturbed deep-ocean barotropic Kelvin wave, the theoretical relation between the particle velocity of the tidal wave u and the sea level elevation η is

$$u = \eta\sqrt{\frac{g}{H}},$$

where g is the earth gravity and H the ocean depth of about 5000 m. The calculated particle velocities are given in column 4 of Table 2. The agreement between observed and calculated particle velocities

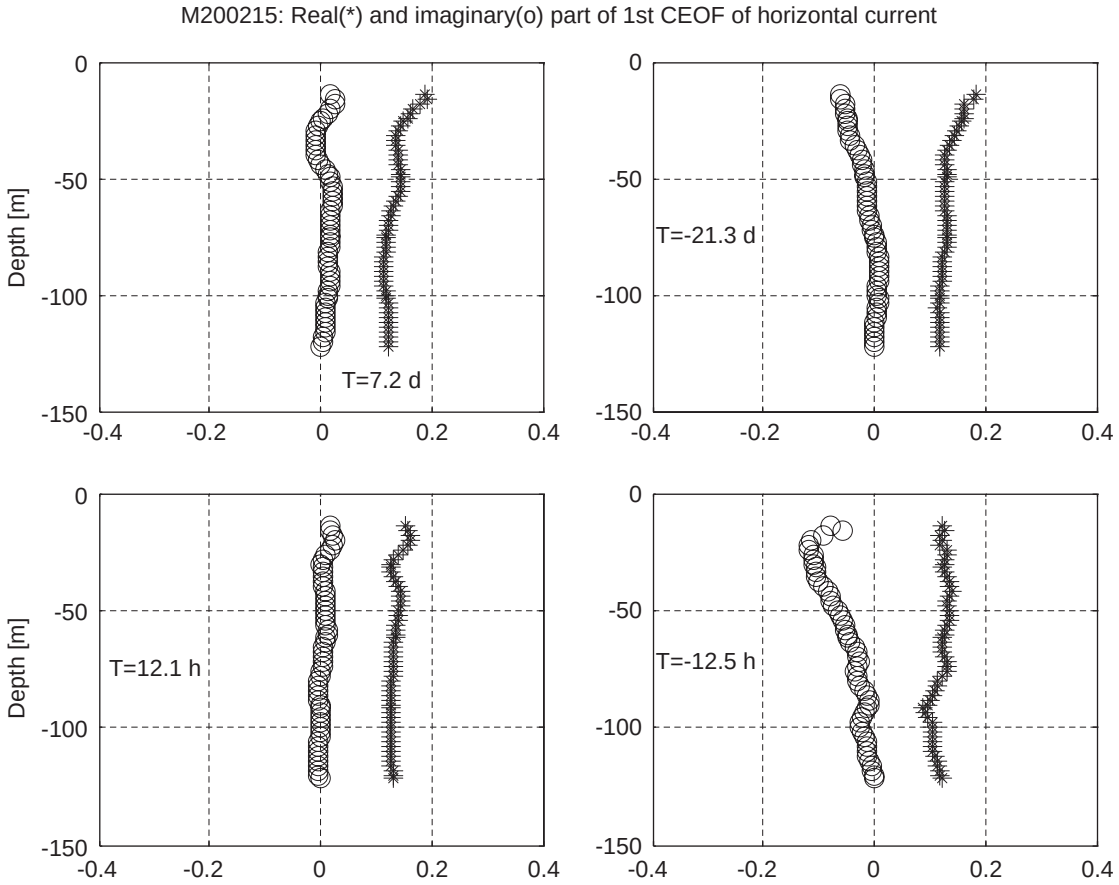

Fig. 8. First vertical eigenfunction of the CEOF analysis at selected periods.

is quite good for the semi diurnal tide while the theoretical velocities are too low for the diurnal tidal constituents. The main perturbation to a deep-ocean Kelvin wave is the cross-shelf flow reflected by the minor axis of the current ellipse.

3.2.2. *Inertial motions*

The frequency band of inertial oscillations and near inertial waves contains most of the energy of the current fluctuations off Walvis Bay, see Fig. 7. The inertial motions are rotating anti-clockwise, as required for the southern hemisphere, and comprise several significant vertical modes. Inertial motions seem to be a substantial part of the flow field in the Benguela, since they were observed along the whole coast of Namibia (Hagen, 1991; Gründlingh, 1999; Simpson et al., 2002), with amplitudes ranging between 10 and 20 cm/s. The vertical structure of the first vertical mode is shown for three frequencies in the inertial band in Fig. 9. The first mode is linear decreasing from near the sea surface to the first node in the thermocline. Below the thermocline the first mode is out of phase to the motion in the surface mixed layer. However, it remains not constant in the lower layer but decreases below 70 m depth and becomes virtually zero beneath 100 m depth. The significance of the higher vertical modes in the inertial wave band suggests vertical propagating phases. The analysis of the current measurements by rotary spectra with respect to the vertical wave number revealed stronger anti-clockwise energy

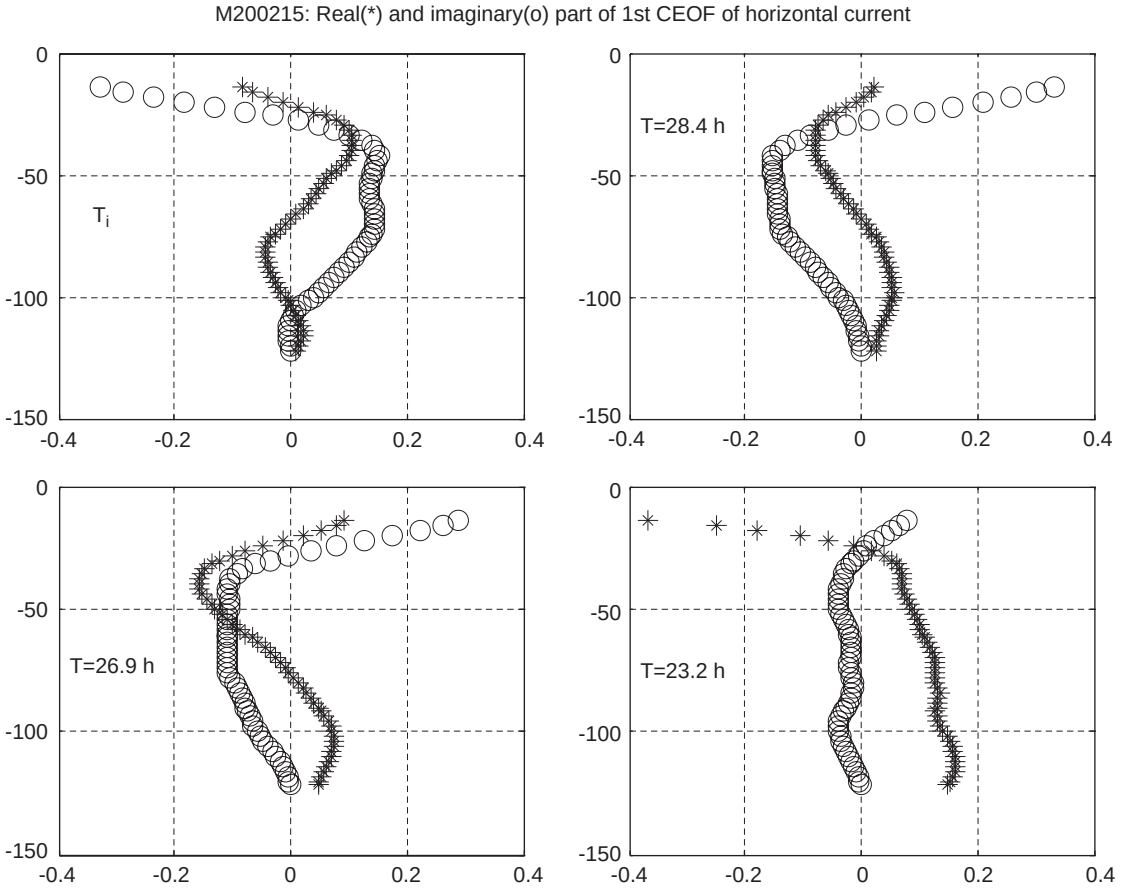

Fig. 9. First vertical eigenfunctions of the CEOF analysis in the inertial wave band and the diurnal tide band.

Table 2
Amplitudes of sea level oscillations, major and minor axis of the current ellipses for the significant tidal constituents at Walvis Bay

Tide	Ampl. (m)	Major (cm/s)	Kelvin wave (cm/s)	Minor (cm/s)	Period (h)
O1	0.018	0.25	0.08	0.08	25.82
K1	0.044	0.60	0.2	0.54	23.93
N2	0.113	0.33	0.5	0.18	12.66
M2	0.522	2.05	2.3	1.21	12.42
S2	0.217	0.88	0.96	0.66	12.00

levels (looking downward from the sea surface) for vertical wave lengths larger than 50 m and equal energy levels for clockwise and anti-clockwise motion for smaller vertical wave length. This suggests that vertical propagating phases are equally distributed between upward and downward propagation at higher modes. Fig. 10 demonstrates the coexistence of up- and downward propagating phases of inertial motions. Since upward/downward phase propagation means downward/upward group velocity of internal waves, this may be an indication that inertial motions are generated near the sea surface as well as near the bottom on the shelf off Walvis Bay.

In order to study the relation between inertial motions and both the wind and the subinertial currents, the amplitude of the first mode of the inertial motion was estimated from the current by projecting the corresponding vertical eigenfunction at the inertial period on the vertical current

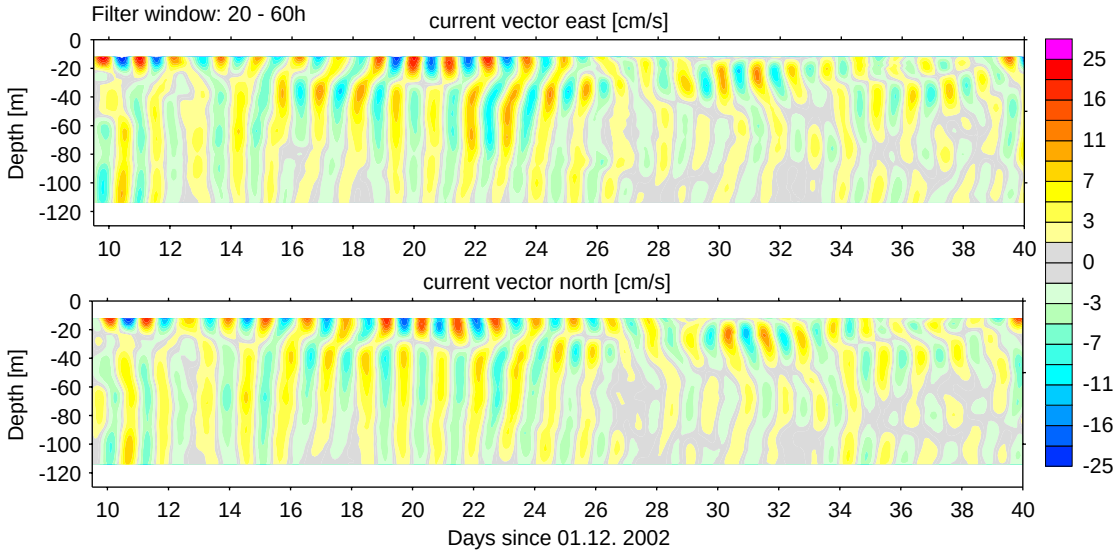

Fig. 10. Bandpass filtered time series of current for the inertial wave band.

profile. The time series of the amplitude depicts temporal variations, which do not correlate with the local subinertial currents but correlate marginally with the variations of the meridional wind stress off Walvis Bay, Fig. 11. The correlation coefficient between both variables is 0.3, which is significant with 95% probability at 45 effective degrees of freedom while 54 effective degrees of freedom were available by these time series.

3.2.3. *Continental shelf waves (CSW)*

The motion in the CSW band centred at the period of about 7.2 days is a pure barotropic one according to both the spectrum of the eigenvalues, Fig. 7, and the structure of the corresponding vertical eigenfunction, Fig. 8. The current measurements were vertical averaged and the resulting barotropic current was analysed with vector spectral analysis. The barotropic motion in the CSW band was significantly anticlockwise rotating while the motion at longer time scales tended to be linear polarised. Moreover, the eccentricity of the rotating current vector in this band was rather large with a ratio of the minor to major half axis of the current ellipse of about 0.4. The major axis was aligned toward north.

CSW's are mainly barotropic and satisfy the rigid lid condition when the width of the continental margin is wide with respect to the internal Rossby radius and small to the barotropic Rossby radius, respectively. This is true for the continental margin off Walvis Bay where the width is about 700 km. CSWs possess a modal structure in offshore direction and each mode has a maximum frequency depending on the depth profile of the shelf (LeBlond and Mysak, 1978). In order to obtain the structure and the possible frequency range of the CWS modes at the shelf off Walvis Bay the differential equation of free CSW was approximated by central difference scheme. The resulting homogeneous linear equations were solved for the eigenfrequencies and eigen functions in a suitable range of wave numbers by means of Matlab routines. The obtained dispersion relations of the first four modes, Fig. 12, reveal a minimum period at about 2, 5.2, 6.5 and 8.1 days for the modes 1–4. This indicates that the first three modes of the CSW's are contributing to the current fluctuations at the shelf off Walvis Bay. Hagen et al. (1981) estimated the dispersion relations of barotropic CSW at the Namibian shelf off 20°S and obtained quite similar results. They found zero group velocity of the third CSW

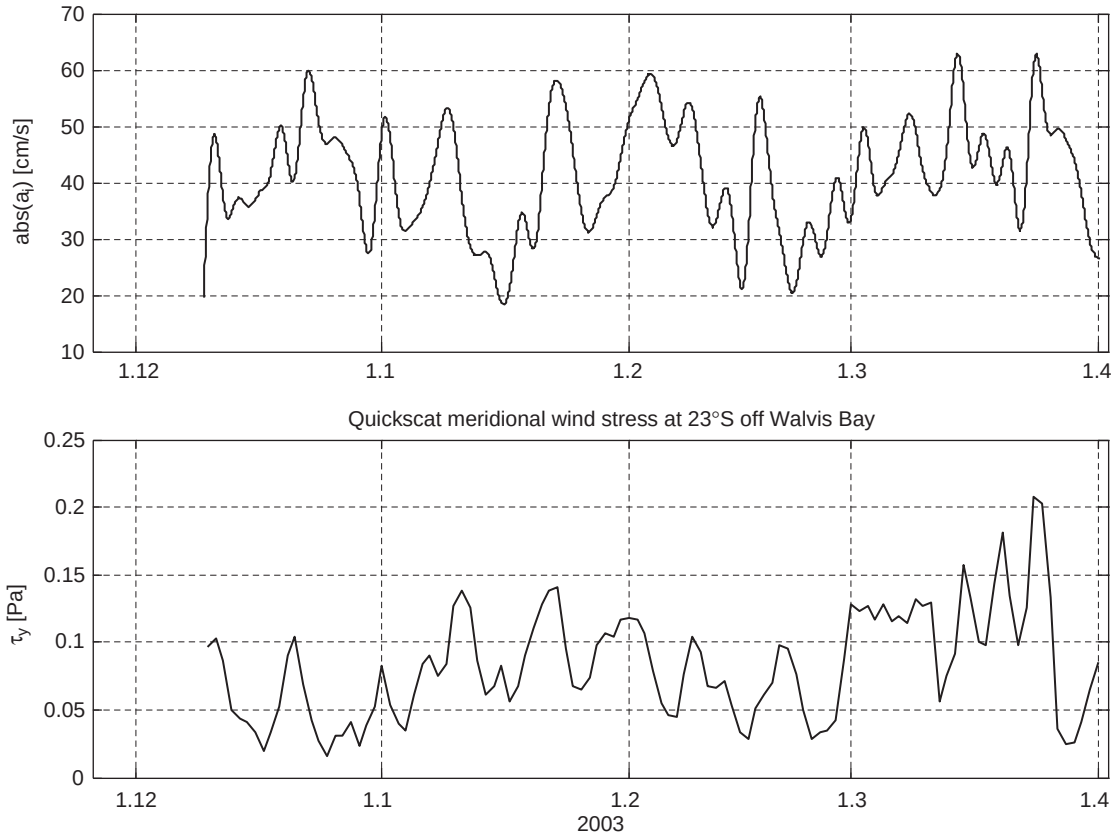

Fig. 11. Absolute amplitude of the first vertical eigenfunction at the inertial period (upper panel) low pass filtered with a 3 d cutt-off period and meridional wind stress off Walvis Bay (lower panel) derived from 3-day averaged QuikSCAT wind data.

mode at the period 7.2 days. The eigenfunctions of the CSW modes depend on wave number and become more trapped at the shelf at higher wave numbers. The eigenfunctions which are proportional to the offshore component of the mass transport are shown in Fig. 13 at wave numbers with maximum frequency of the corresponding mode (zero group velocity). They show that the maximum of the mass transport is located at the maxim shelf slope and that several nodes of the eigenfunctions occur between the coast and the shelf edge. Evidence for such properties of the zonal mass transport off Walvis Bay was found on several LADCP sections along 23°S, for location see Fig. 1. A typical pattern of the measured zonal component of the current is shown in Fig. 14. For a comparison between LADCP measurements and theoretical eigenfunctions one has to take into

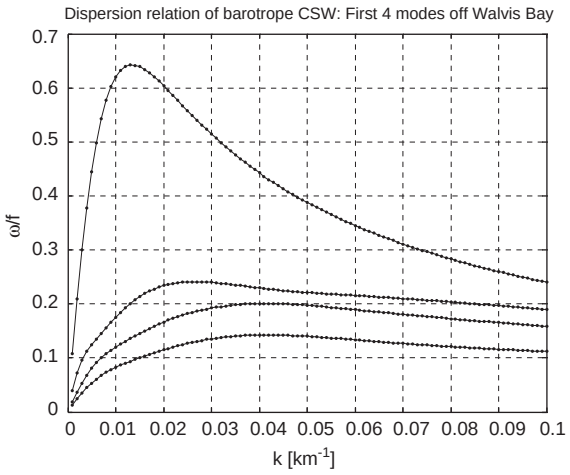

Fig. 12. Dispersion relation of barotrope Continental Shelf Waves off Walvis Bay for mode numbers one (highest frequency) to four (lowest frequency).

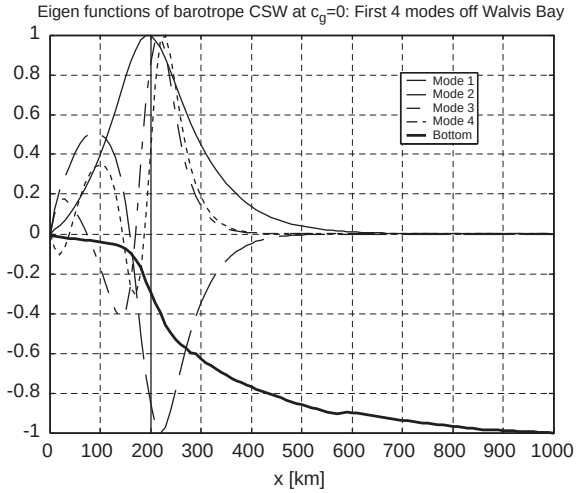

Fig. 13. Eigenfunctions of the first four modes of the barotrope CSW at zero group velocity on the shelf off Walvis Bay. The eigenfunctions are proportional to the offshore mass transport. The derivation of the eigenfunction with respect to the offshore coordinate is proportional to the negative longshore transport.

account that different modes of CSW's and inertial motions superimpose each other which makes a direct comparison difficult.

The low pass filtered meridional component of the barotropic current is shown in Fig. 15. This current exhibits variations with the time scale of about 7 days, as revealed by the spectral analysis. However, these fluctuations are non-stationary since they are well pronounced in December 2002 and March 2003 but weak in between. During these phases they are correlated with the meridional wind stress off Walvis Bay. The meridional current exhibits fluctuations with a time scale of a month as well which are not resolved by our spectral analysis. Two phases of well-pronounced poleward current were observed which lasted for about 1 month each. The first phase went from mid December 2002 till mid January 2003 and the second phase lasted from mid January till mid February 2003. Weak poleward current occurred from end of February till end of March. Both phases of well-developed poleward current are associated with periods of calm meridional wind stress at the location of the mooring while the break of the poleward current at mid January 2003 was associated with an intensified meridional wind stress on the shelf off Walvis Bay. Both phases of strong poleward current are also associated with weak meridional wind stress in the area of the Angola-Benguela front, while well developed negative wind stress curl off Walvis Bay and in the area of the Angola Gyre occurs only during the second phase of strong poleward current from mid January to mid February 2003. The wind stress curl is negative at both locations in March 2003. However, during this time the SE Trade strengthened off Walvis Bay and counteracts the forcing of the poleward current by wind stress curl.

3.2.4. Long time scales

In order to study the shelf circulation at longer time scales the mean vertical current profiles averaged over the whole record and progressive vector diagrams were calculated at selected depths. The uppermost depth level measured by the ADCP in 14 m depth was taken as representative for the surface layer. An intermediate depth level was taken at the maximum counter current to the surface layer according to the first CEOF at the inertial frequency in 40 m depth. Additionally, a progressive vector diagram was calculated at 100 m depth where the circulation is quite low according to the 1st CEOF at the inertial oscillation. The progressive vector diagrams at the selected depth levels are shown in Fig. 16. They show that the surface layer is rather decoupled from the layers below the thermocline. The motion in the surface layer is dominated by inertial motions while the deep layers are dominated by the poleward current with fluctuations already described above. With respect to the cross shelf circulation the progressive vector diagrams depict a three-layer pattern. The surface layer moves offshore as expected according to the Ekman current. The intermediate layer moves as a corresponding compensating current in onshore direction, while the water in the bottom layer moves offshore as in the surface layer. The structure of the cross shelf circulation is depicted more precisely by the mean meridional component shown in Fig. 17. The Ekman current is restricted to the surface layer above 15 m depth. The onshore compensation current is sandwiched in an inter-

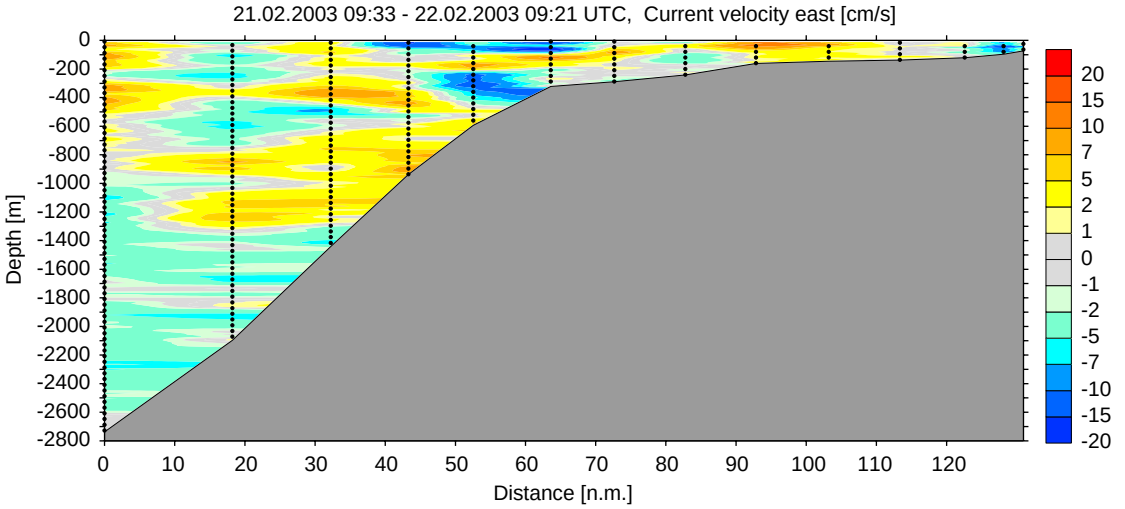

Fig. 14. Zonal component of current measured by LADCP on a section off Walvis Bay at 23°S.

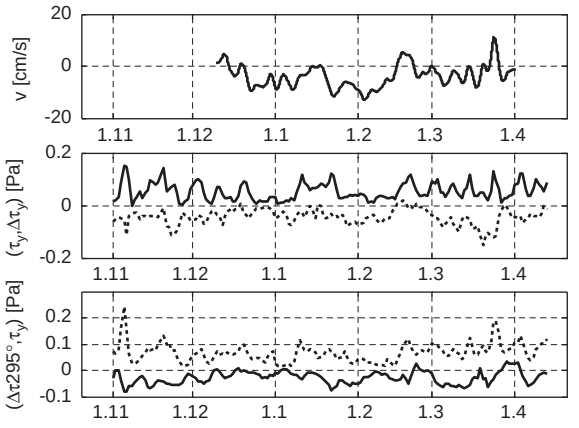

Fig. 15. Low-pass filtered (Tc = 3 days) meridional component of the barotropic current at M200215 (upper panel). The middle panel shows the meridional component of the wind stress at the mooring position (solid line) and the zonal difference of the meridional wind stress between 14°E and 12°E at 23°S as measure of the wind stress curl off Walvis Bay (dashed line). The difference of the wind stress projected onto the direction toward 295° between 8°S, 1.4°E and 15°S, 2°W is shown in the lower pane (solid line). This difference is a measure of the wind stress curl in the area of the Angola Gyre. The meridional wind stress in the Angola-Benguela front area at 11°E (dashed line) is shown in the lower panel as well. The wind stresses in this figure were derived from 3-day averaged QuikSCAT wind measurements.

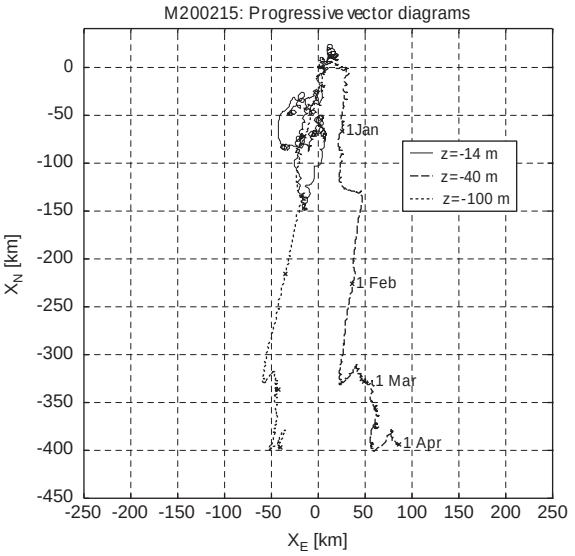

Fig. 16. Progressive vector diagrams at selected depth levels of the current profile.

mediate layer between 15 and 70 m depth while the offshore current in the bottom layer increases from 70 m depth toward the bottom. The vertical structure of the cross circulation agrees in principle with the real part of the 1st EOF in the inertial

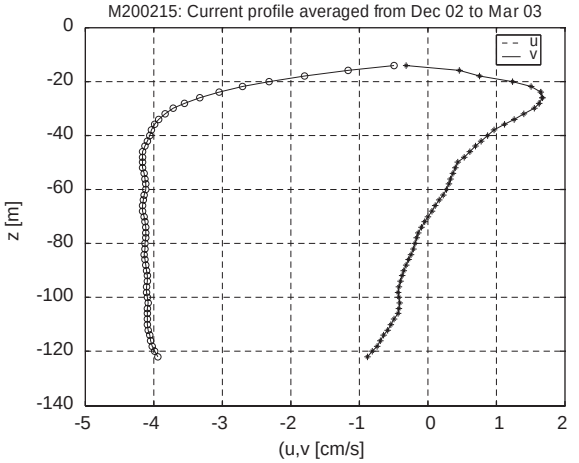

Fig. 17. Mean profile current of current components averaged over the complete measurement period.

frequency band, see Fig. 9, except for the bottom layer where the real part of the EOF approaches to zero, in contrast to the mean meridional component, see Fig. 17. The amplitude of the mean cross shelf circulation is about 1 cm/s.

The mean longshore current has a two layer structure. The wind driven surface current is observed in the upper 30 m of the water column and the poleward current is rather constant below 30 m depth with a mean velocity of 4 cm/s.

3.2.5. *Wind current correlation*

An attempt was made to analyse the relation between the current and the local wind measured at the meteorological buoy off Swakopmund, which was separated by a distance of about 30 nm from the current meter mooring. Since the horizontal scales of the meteorological processes which force the ocean are much larger compared with this distance the wind measured off Swakopmund may represent to a large extend the local wind at the mooring position.

The measured current was high pass filtered by a 4th order Butterworth filter with a cut off period of 72 h in order to analyse the relation between the wind and the current fluctuations in the inertial and tidal bands. The vertical eigenfunctions of the filtered currents and their corresponding amplitudes were estimated by an EOF analysis in the time domain. The eigenvalues of the first three vertical modes were significantly different from noise. The first vertical eigenfunction had a structure of a first baroclinic mode. An invariant cross spectral analysis between the pseudo wind stress vector measured at the meteorological buoy off Swakopmund and the vector amplitude of the first vertical mode was performed according to Mooers (1973). The length of the record was 2710 while the number of frequency bands was 256. This results in a level of significance for the coherence of 0.46 with a 90% probability.

Significant coherence between the current and the pseudo wind stress was found only for the amplitude of the first vertical eigenfunction at the diurnal period, see Figs. 18 and 19. The anticlockwise component of the current was significantly coherent with both the clockwise and the anticlockwise component of the pseudo wind stress. The pseudo wind stress led the current by about 90° (6 h) on both components. The transfer coefficient between the amplitude of the first mode of the current and the wind stress was of the order 10^3 cm/s/Pa. The typical amplitude of the diurnal wind fluctuation is 3 m/s. This results in a diurnal current fluctuation of about 5 cm/s close to the sea surface according to the transfer coefficient. There was no significant coherence between the clockwise component of the current and the pseudo wind stress at the diurnal period.

The coherence at the inertial period exhibits a small peak, which was just below the level of significant coherence. This lack of significant coherence between the wind and current at the inertial period may be due to the superposition of inertial motions forced by the local wind stress and propagating inertial waves which were forced at distant locations. The latter represent noise to the locally forced inertial motions.

The relation between the wind and the barotropic component of the current was analysed for the full spectrum resolved by the measurements. The barotropic component of the current is not, or at least marginally coherent with the local wind at periods larger than 3 days. A visual inspection of the low-pass filtered time series of the meridional components of both the pseudo wind stress and the current revealed that a coherence between the

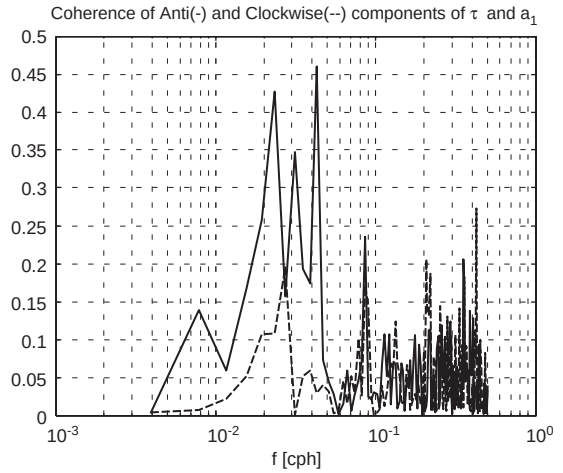

Fig. 18. Coherence between pseudo wind stress at the moored buoy off Swakopmund and the amplitude of the first vertical EOF of the high-pass filtered current off Walvis Bay. The solid line represents the coherence between the ant-clockwise components and the dashed line the coherence between the clockwise components, respectively. The level of significant coherence is 0.46 and 0.52 for 90% and 95% probability, respectively.

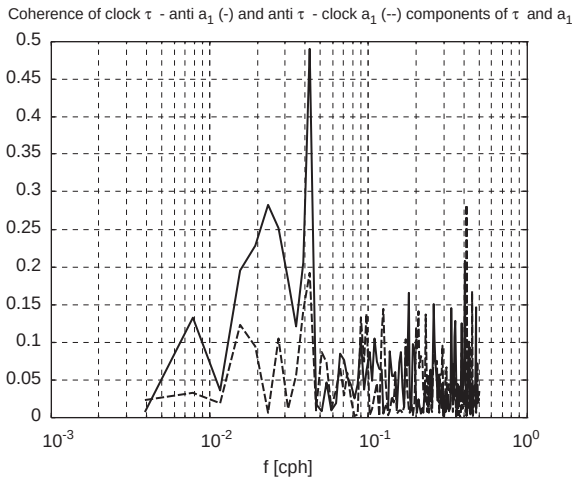

Fig. 19. Coherence between pseudo wind stress at the moored buoy off Swakopmund and the amplitude of the first vertical EOF of the high-pass filtered current off Walvis Bay. The solid line represents the coherence between the clockwise component of the wind stress and the ant-clockwise component of the current and the dashed line the coherence between the opposite components, respectively. The level of significant coherence is 0.46 and 0.52 for 90% and 95% probability, respectively.

current and the local stress wind vector occurred only during a small fraction of the whole record, namely in the later half of March 2003, while for the other periods the current was governed by free Kelvin waves and currents forced by the curl of the wind stress.

3.3. Temperature and water masses

The time series of temperature profiles measured at the mooring were analysed by means of the complex EOF analysis as described in Section 2.5. The spectrum of eigenvalues of the three most energetic modes is shown in Fig. 20. The spectra generally decrease with frequency except for the first and third modes which both depict a small peak around the local inertial frequency f_i. The vertical eigenfunctions of the first modes at the most energetic frequency $f = 0$ and at the inertial frequency f_i are shown in Fig. 21. The first eigenfunction at the low frequency end of the spectrum describes that the temperature changes at these frequencies comprise the whole water column with equal phase but different intensity. The temperature changes are biggest in the surface mixed layer, which extends over the upper 25 m and decrease continuously below the mixed layer toward the bottom where they account for about

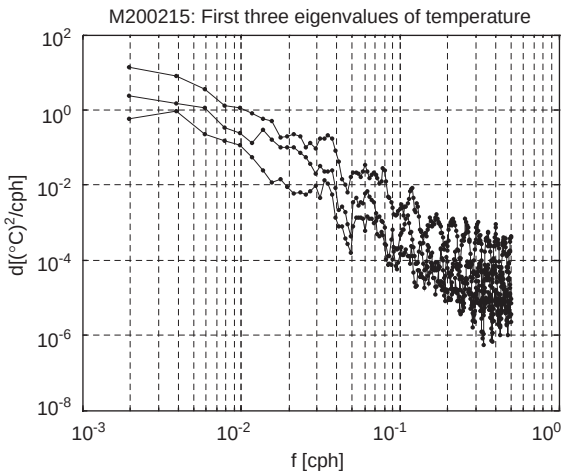

Fig. 20. Spectrum of the first three eigenvalues of the temperature profiles measured at the mooring M200215.

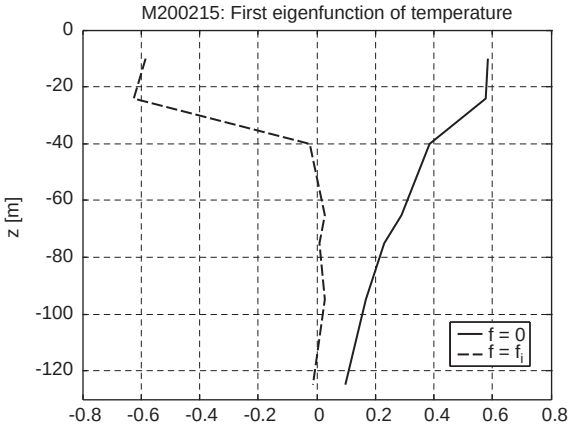

Fig. 21. First vertical eigenfunctions of the temperature profile measured at the mooring M200215. The eigenfuction at zero frequency is represented by the solid line and at the inertial frequency by the dashed line, respectively.

20% of the variability in the surface mixed layer. The first vertical eigenfunction at the inertial frequency has a maximum in the thermocline and decreases toward the sea surface and larger depths. This eigenfunction is all but zero at depths below 60 m. The eigenfunction of the third mode at f_i is almost zero below 90 m depth and has a maximum close to 60 m depth, which is in phase with a maximum in the surface mixed layer and out of phase with a maximum in the thermocline.

Two main water masses are observed on the Namibian shelf, the South Atlantic Central Water (SACW) and the Eastern South Atlantic Central Water (ESACW). The SACW is the tropical type of central water, which is transported southward from the Angola Gyre by the Angola Current and the poleward undercurrent. ESACW is transported northward with the Benguela Current off the shelf and linked to the shelf with the compensation current associated with the wind driven Ekman current in the surface mixed layer (for details see Mohrholz et al., 2001). The mooring was positioned in an area where both water masses are mixed. Below the surface mixed layer temperature and salinity are assumed to be conservative parameters. The fraction of SACW was calculated using the definition of SACW by Hagen and Schemainda (1987) and that of ESACW by Poole and Tomczak (1999).

The general trend of the water mass changes on the shelf off Walvis Bay during austral summer 2002–2003 was that the water became warmer and saltier, in particular after February 2003, see Fig. 22. This indicates an increasing fraction of SACW on the shelf. The fraction of SACW was calculated from the Seacat measurements at 65 and 125 m depth, respectively. Both instruments featured a sufficient accuracy to perform these calculations. Generally, the SACW had a higher percentage in the water close to the bottom at 125 m depth than in the water at an intermediate depth (65 m) Fig. 23. However, the SACW fraction was increasing during the whole phase from December 2002 to end of March 2003. The bottom layer is better resolved by the CTD measurements repeatedly taken along the section shown in Fig. 1. The density profiles shown in Fig. 24, reveal the existence of a mixed bottom layer which is up to several 10 m thick. This layer was observed not at every station but very frequent on the shelf and less frequent at the shelf slope. Oxygen concentration is spurious only within this layer on the shelf but is increasing toward the shelf edge, see Fig. 25. The turbidity, not shown here, was generally increasing toward the bottom within the bottom mixed layer on the shelf compared with the turbidity in the intermediate layer above. Occasionally, a constant high turbidity was observed within the bottom layer.

4. Discussion

The temporal variations of the current field on the shelf of the South East Atlantic off Walvis Bay were studied during austral summer and fall by moored current profiler and temperature salinity recorder. The upward looking RDI 300 kHz WH ADCP was located close to the bottom and provided hourly current profiles with 4 m vertical resolution between a few metres above the bottom and close to the surface. The four Seacat TS recorders and three Seamon temperature recorders provided hourly temperature profiles at 7 and salinity at 4 discrete depth levels, respectively,

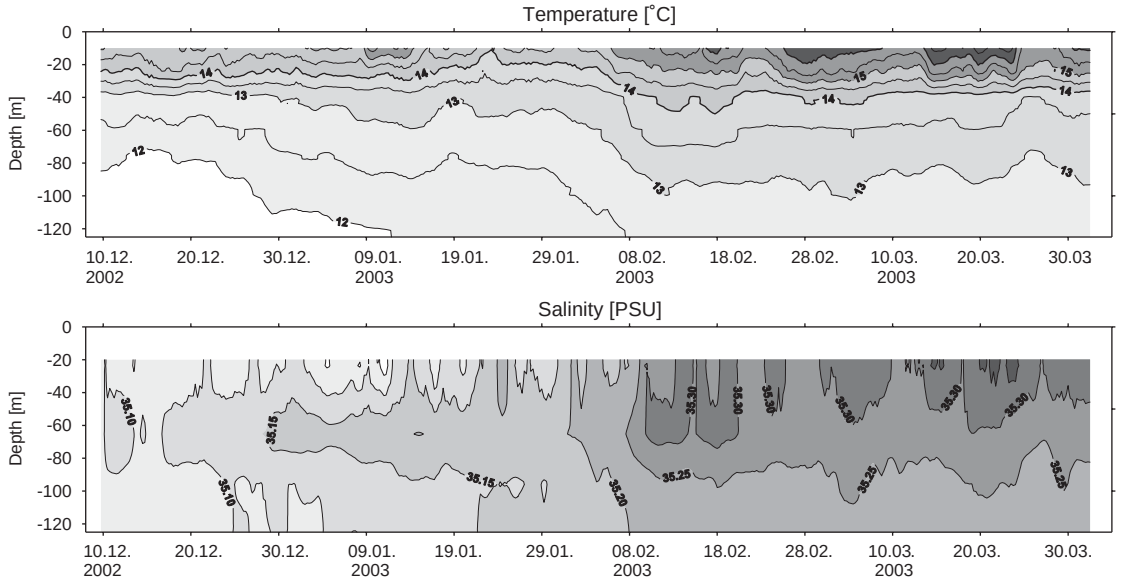

Fig. 22. Time series of temperature (upper panel) and salinity (lower panel) at the mooring position off Walvis Bay.

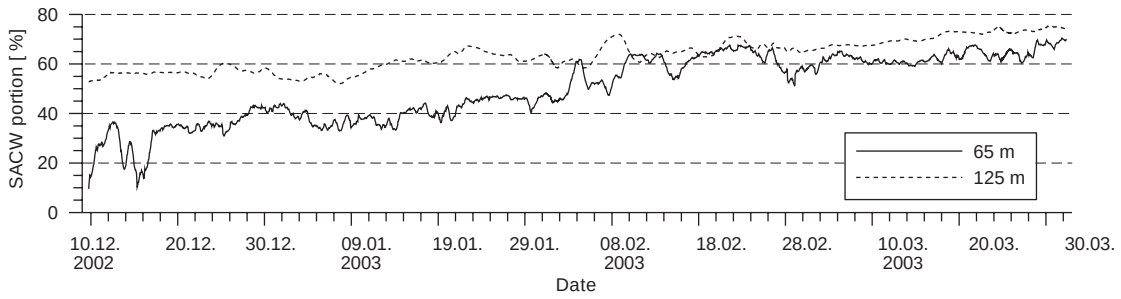

Fig. 23. Time series of SACW content on the shelf off Walvis Bay in 65- and 125-m depth.

which were distributed over the whole water column. Spatial and temporal variations of the wind field in the South East Atlantic were studied by 3-day averaged wind fields measured by the QuikSCAT satellite and the local wind was provided by a time series of hourly wind vectors measured on a moored buoy off Swakopmund.

The significant tidal motion on the shelf off Walvis Bay is composed by the semidiurnal constituents M2 and S2. This motion is a barotropic anti-clockwise rotation of the current vectors on ellipses whose main axes are oriented along the coast. The relation between the minor axis and the major axis of the ellipses are 0.6 and 0.75 for the M2 and S2 tide, respectively. The velocities of the major axes are 2.05 and 0.9 cm/s for the M2 and S2 constituents, respectively. These current velocities correspond to the velocities of a barotropic deep ocean Kelvin wave in a first order.

The currents in the diurnal band were governed by an anti-clockwise oscillation forced by both the anti-clockwise and clockwise rotating components of the local land-sea breeze. The current has a two layer structure consisting of a surface layer attributed to the mixed surface layer and an almost evenly distributed deep layer which is in

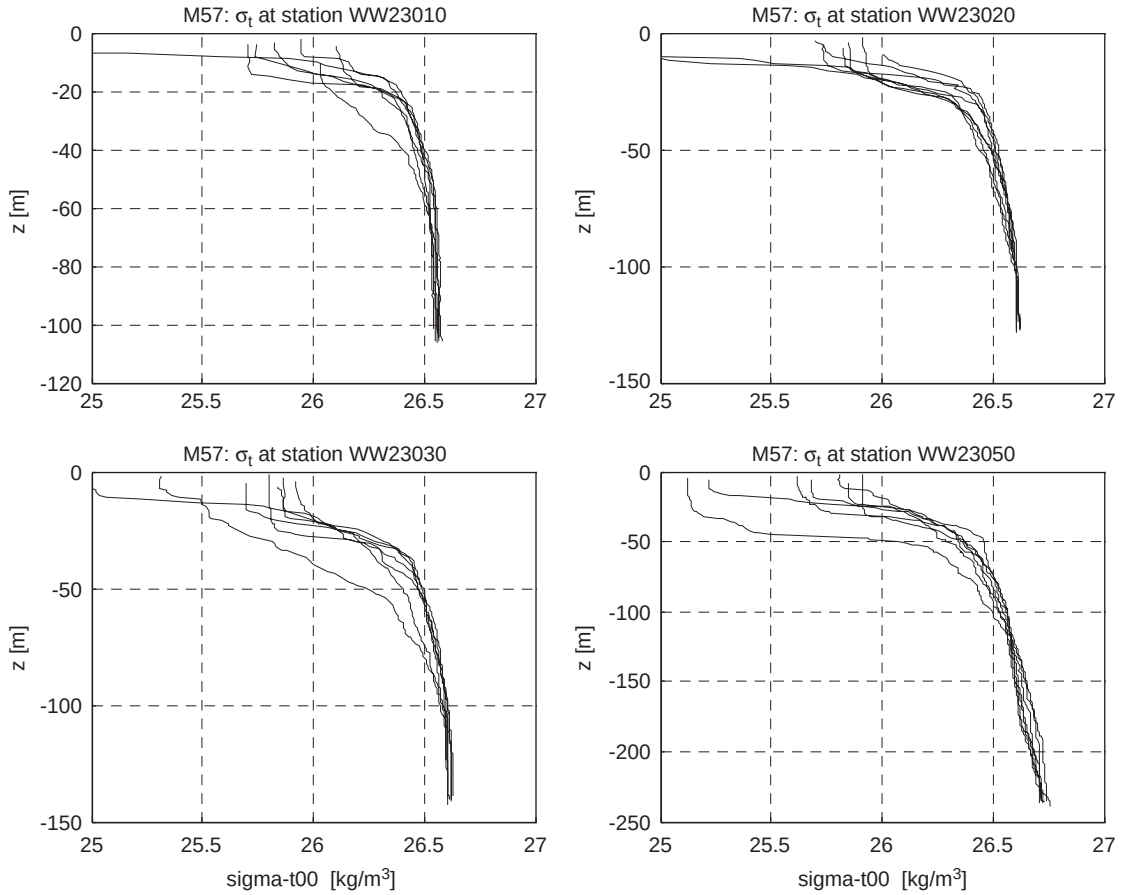

Fig. 24. Vertical density profiles measured during February to March 2003 on the shelf and at the shelf edge (WW23050) off Walvis Bay. See Fig. 1 for the positions of the stations.

opposite direction to the surface layer compensating the mass flux in the surface layer.

Most of the energy of the current fluctuations were concentrated in the frequency band corresponding to the local inertial period of $T_i = 30.7$ h. These fluctuations consisted of at least four significant anti-clockwise rotating vertical modes with resulting characteristic amplitudes ranging between 10 and 20 cm/s. This suggests that the inertial motions consist of a superposition of inertial oscillation and near inertial waves. The near inertial waves contributed to the temperature fluctuations in the upper 60 m of the water column. The superposition of the higher vertical modes appeared with an equally distributed upward and downward phase propagation averaged over the interval of observation. This implies that inertial waves were generated in the surface layer as well as in the bottom layer. According to linear theory, e.g. Fennel and Lass (1989), the inertial motion consists shortly after the onset of a generating wind of an inertial oscillation in the surface mixed layer superimposed by a barotropic inertial wave propagating from the coast into the open sea. The vertical structure of the resulting inertial motion behind the front of the seaward propagating barotropic inertial wave consists of a reduced inertial motion in the surface mixed layer and a compensating inertial motion below the mixed layer which compensates the mass flow in the

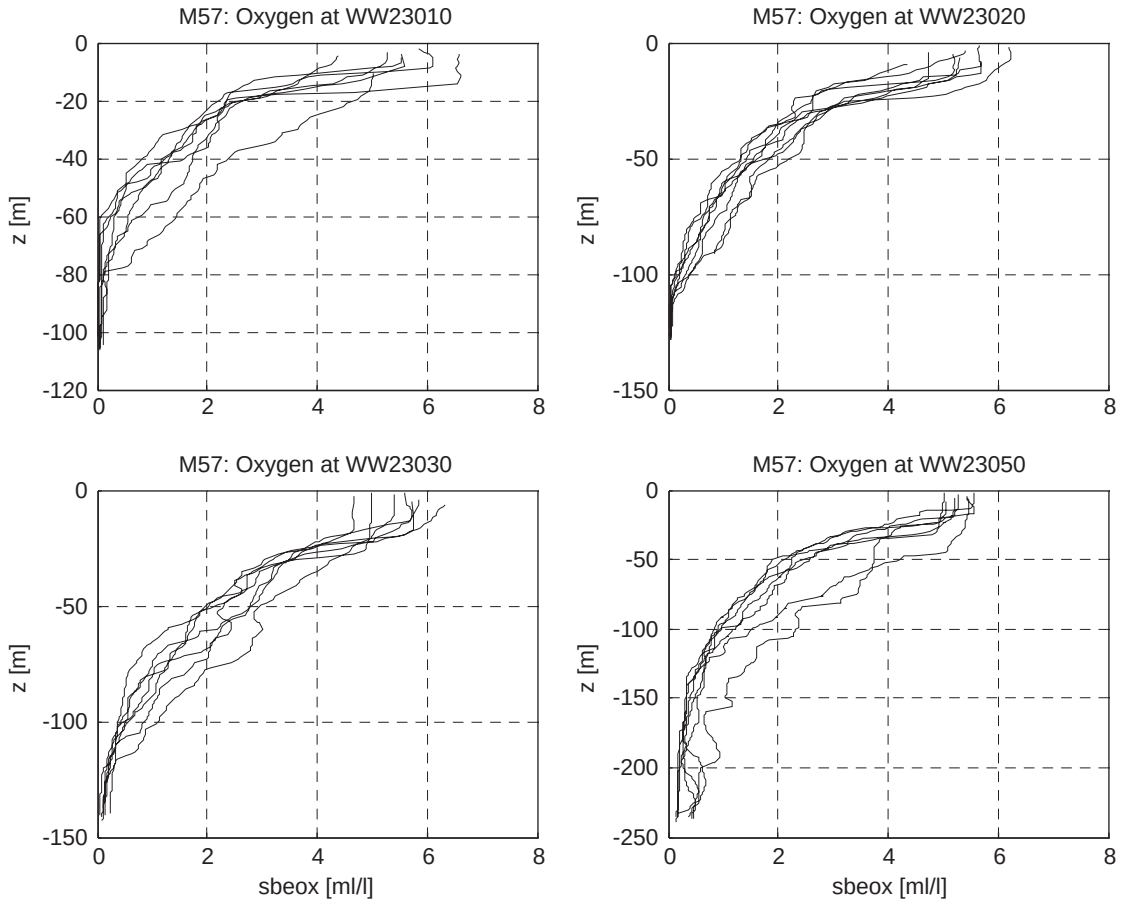

Fig. 25. Vertical profiles of oxygen concentration measured during February to March 2003 on the shelf and at the shelf edge (WW23050) off Walvis Bay. See Fig. 1 for the positions of the stations.

surface mixed layer normal to the coast. This kind of structure should be reflected in the first vertical mode of the inertial motion. The observed vertical structure in the first vertical mode differed from the theoretical model below the surface mixed layer where the observed structure was not constant but dropped to zero between 70 and 100 m depth and remained almost zero below 100 m depth. Since the inertial motions control the transition into the stationary Ekman current one can expect that the vertical structure of the cross shelf circulation is similar to those of the inertial motions. This suggests that the compensation current to the wind driven Ekman current in the surface mixed layer occurs in an intermediate layer between the mixed layer and a bottom layer as described by the first vertical mode of the inertial motion. A similar structure of the first vertical mode of the inertial motion was observed in the Baltic Sea (Lass et al., 2003). A possible reason for this kind of vertical structure could be interaction between the barotropic and the baroclinic modes in stratified water on the inclined shelf. This mode interaction is the process, which transfers energy from the barotropic to the baroclinic inertial waves. It is interesting to note that only the inertial motion has a kind of bottom boundary layer, see Fig. 9 upper left panel, which extends over the same depth range of about 30 m above the bottom as the bottom mixed layer depicted by the

vertical density profiles shown in Fig. 24. This layer may be a shadow zone for inertial waves since its Brunt-Väisälä frequency is close to zero. It is not clear which process provides the turbulent energy for the mixing of this layer since a typical turbulent bottom friction layer would require a vertical current shear independent of the time scale of the process inducing the bottom current, e.g. tides or CSW's. One might speculate that differential advection according to van Aken (1986), which is due to the combined action of the cross shelf density gradient and the vertical shear of the circular polarised inertial current, could be a possible candidates for the mixing of the bottom layer because this mechanism occurs on the shelf as well as on the shelf slope.

The correlation between the local wind and the inertial motion was just below the level of significance at 95% probability. The kinetic energy of the inertial motions on the shelf correlated also marginally with the meridional component of the wind stress off Walvis Bay, indicating that both the local wind and the radiation of remotely generated inertial waves determine the inertial motions off Walvis Bay.

Energetic subinertial current fluctuations were observed in a frequency band centred at a period of 7.2 days. These fluctuations consisted of one significant vertical mode only which possessed a rather barotropic structure with a slight enhancement in the surface mixed layer. The barotropic motions in this frequency band were rotating anticlockwise on an eccentric ellipse whose major axis was aligned along the coast. The coherence between the barotropic current and the sea level was significant for periods in the M2 band and for periods larger than 7 days. Current and sea level were in phase in the tidal band and out of phase in the low frequency band. There was no significant coherence between the local wind stress and the motions in the 7 days band. This suggests that these motions consist of the superposition of locally forced fractions and free Continental Shelf Waves radiated from remote distances. Continental Shelf Waves with time scales of 7 days exist only for horizontal mode numbers of less than four according to dispersion relations estimated for the shelf off Walvis Bay.

The longshore circulation of the Benguela system consists, according to the linear theory of Fennel (1999), of a wind driven coastal jet in the surface layer and a poleward undercurrent below the surface mixed layer which both taper off toward the Angola-Benguela front due to the Kelvin waves propagating poleward from this front. The wind stress curl in the Benguela produces a secondary divergence of the offshore Ekman transport and forces upwelling and a downwind surface flow in the offshore area and a counter current in a coastal strip. The latter can be stronger than the surface jet in the northern Benguela resulting in a poleward surface current. Observations have shown that pulses of poleward flow in the whole water column, starting from the area just north of the Angola-Benguela front, can penetrate into the Benguela as Kelvin wave. These pulses are forced by fluctuations of the wind stress curl in the area of the Angola Gyre (Lass et al., 2000) or by a sudden relaxation of the meridional wind stress in the northern Benguela (Mohrholz et al., 2001).

The observed longshore current on the shelf off Walvis Bay consisted of a superposition of an equatorward wind driven surface layer and a barotropic polward current. The barotropic fluctuations had a time scales of the order of 1 month which could not be resolved by spectral methods of the measured time series. Two phases of poleward current on this time scale occurred during the period of observation. The first one occurred from mid December 2002 to mid January 2003 and the second one from mid January to mid February 2003. During the first phase both the local and the meridional wind stress at the Angola-Benguela front as well as the local curl of the wind stress were weak. During the second phase both the local and the meridional wind stress at the Angola-Benguela front were weak likewise but the local curl of the wind stress was significantly negative forcing a poleward current according to Fennel (1999). Both phases were separated by a positive pulse of local meridional wind stress. This suggests that the first phase of the poleward undercurrent consisted of a free Kelvin wave propagating from the area of elevated sea level north of the Angola-Benguela front while the

second phase of the undercurrent was additionally forced by the local negative wind stress curl off Walvis Bay. Negative wind stress curl was present together with a equatorward local wind stress from end of February to end of March 2003. This resulted in a weak mean poleward current, which was interrupted by equatorward directed current pulses forced by northward wind stress pulses.

The cross shore circulation depicted a two cell pattern. The surface layer coincided with the Ekman offshore current, which was compensated by an onshore current in an intermediate layer below the surface mixed layer and 70 m depth while the bottom layer was exposed again to an offshore current. This has dramatic consequences for the ventilation of the shelf water below the thermocline, which is ventilated by onshore current in the intermediate layer but practically not ventilated in the bottom layer. The existence of the bottom cell of the cross circulation can be understood either in terms of an Ekman bottom friction layer or in terms of a baroclinic longshore pressure gradient which compensates the barotropic longshore pressure gradient at the bottom of the intermediate layer. However, the Ekman spiral in the bottom friction layer should result in a reduced longshore current in the depth range where the offshore circulation develops. Similarly, the geostrophic offshore current, resulting from an equatorward baroclinic pressure gradient force due to water of higher density at Lüderitz and lower density at the Angola-Benguela front, should force a corresponding reduction of the poleward undercurrent in the bottom layer. This reduction of the longshore current was not in the depth range of the bottom cross circulation cell. Hence, its physical nature remains unexplained.

The SACW advected by the poleward current, at least in the whole water column below the mixed layer, and the ESACW advected toward the shore by the cross shelf circulation in the intermediate layer below the surface mixed layer are mixed together at the shelf according to their advective flux. The concentration of the shoreward cross shelf circulation on the intermediate layer results in a higher contribution of ESACW fraction in the intermediate layer compared to the bottom layer. This 10–30 m thick bottom layer was well mixed on the shelf and extremely depleted of oxygen indicating that the balance between ventilation by mixing and advection and oxygen consumption was displaced to the latter one compared to the ambient regions. Generally, there was an increase in the SACW fraction in the whole water column in austral summer and fall due to the stronger advection by the poleward undercurrent in this season.

5. Conclusions

The conclusions are based on the analysis of current, temperature and salinity observations at a single mooring on the shelf off Walvis Bay at a water depth of about 130 m together with satellite and moored wind measurements. The measurements were performed in austral summer und fall and revealed:

- The barotropic S2 and M2 tidal constituents dominated the anticlockwise tidal motions on the shelf off Walvis Bay. The amplitudes of these motions correspond to those of a barotrope deep ocean Kelvin wave in a first order.
- The anticlockwise diurnal motion is driven by the land-sea breeze in the surface mixed layer with a compensating current in the deep layer.
- The anticlockwise inertial motions are the most energetic motions on the shelf. They consist of a superposition of inertial oscillations and both locally as well as remotely forced near inertial waves, which are generated as well near the sea surface as near the bottom. These motions are most pronounced in both the surface and the intermediate layer and disappear virtually in a 30 m thick bottom layer.
- Barotropic coastal trapped waves with a period of about 7 days were found. The waves were of horizontal mode number less than four.
- The longshore circulation was governed by a superposition of a wind driven equatorward jet and a barotropic poleward counter current due to the negative wind stress curl off Walvis Bay and a free Kelvin wave, which likely emanated from the Angola-Benguela front.
- The cross shore circulation consisted of a two cell pattern. The upper cell was driven by the

Ekman offshore transport in the surface layer complemented by an onshore compensation current in the intermediate layer below the thermocline and 70 m depth. An additional offshore current was found in the bottom layer below the intermediate layer whose physical nature could not be explained.

- During summer and fall the fraction of SACW on the shelf was continuously increasing due to the intensified advection by the poleward current and the reduced cross shore circulation in particular in the bottom layer.

Acknowledgements

We greatly acknowledge the qualified support of the Captains, officers and crews of R/V Meteor and R/V Welwitschia during the deployment, maintenance and recovery of the mooring. Günter Plüschke took care in composing and assembling the mooring and Toralf Heene skilfully prepared and maintained the deployed instruments and processed the recovered data. Ekkehard Klingelhöffer and Anja van der Plas, at NatMIRC, generously provided a marker buoy and informed the local fishing fleet on the deployment of the mooring which helped to avoid conflicts between the mooring and fishery vessels. Chris Bartholomae kindly provided the time series of wind vectors measured on the meteorological buoy off Swakopmund owned by NatMIRC and on the NatMIRC building in Swakopmund. The tide gauge record at Walvis Bay habour was gently provided by Aina Iita from NatMIRC Swakopmund, Namibia.

QuikScat data and images are produced by Remote Sensing Systems and sponsored by the NASA Ocean Vector Winds Science Team.

The helpful comments of two anonymous reviewers are acknowledged.

References

van Aken, H.M., 1986. The onset of stratification in shelf seas due to differential advection in the presence of a salinity gradient. Continental Shelf Research 5, 475–485.

Bakun, A., Nelson, C.S., 1991. The seasonal cycle of wind stress curl in the sub-tropical eastern boundary current regions. Journal of Physical Oceanography 21, 1815–1834.

Boyd, A.J., 1987. The oceanography of the Namibian shelf. Ph. D. Thesis, University of Cape Town, 190pp.

Chapman, P., Shannon, L.V., 1985. The Benguela Ecosystem Part II. Chemistry and related processes. Oceanography and Marine Biology—An Annual Review 23, 183–251.

Chapman, P., Shannon, L.V., 1987. Seasonality in the oxygen minimum layers at the extremities of the Benguela System. South African Journal of Marine Science 5, 85–94.

Copenhagen, W.J., 1953. The periodic mortality of fish in the Walvis region. A phenomenon within the Benguela Current. Investl. Rep. Div. Fish. S. Afr., 14, 35pp.

Emery, W.J., Thomson, R.E., 2001. Data Analysis Methods in Physical Oceanography, second and revised ed. Elsevier, Amsterdam, London, New York 638pp.

Fairall, C., Bradley, E., Rogers, D., Edson, J., Young, G., 1996. Bulk parameterization of air-sea fluxes for tropical ocean global atmosphere coupled ocean atmosphere response experiment. Journal of Geophysical Research 101 (C2), 3747–3764.

Fennel, W., 1999. Theory of the Benulea upwelling system. Journal of Physical Oceanography 29, 177–190.

Fennel, W., Lass, H.U., 1989. Analytical Theory of Forced Oceanic Waves. Akademie-Verlag, Berlin 312pp.

Garzoli, S.L., Gordon, A.L., 1996. Origins and variability of the Benguela Current. Journal of Geophysical Research 101, 897–906.

Greiner, E., Arnault, S., 2000. Comparing the results of 4D-variational assimilation of satellite and in situ data with WOCE CITHER hydrographic measurements in the tropical Atlantic. Progress in Oceanography 47, 1–68.

Gründlingh, M.L., 1999. Surface currents derived from satellite-tracked buoys off Namibia. Deep-Sea Research II 46, 457–473.

Hagen, E., 1979. Zur Dynamik charakteristischer Variationen mit barotropem Charakter in mesoskalen ozeanologischen Feldverteilungen küstennaher Auftriebsgebiete. Geodätische und Geophysikalische Veröffentlichungen, R. IV, H. 29, 3–71.

Hagen, E., 1991. Beobachtungen der täglichen und mehrtägigen Auftriebsvariabilität über dem Schelf von Namibia im Herbst 1976. Beiträge zur Meereskunde 62, 3–34.

Hagen, E., Schemainda, R., 1987. On the zonal distribution of South Atlantic Central Water (SACW) along a section off Cape Blanc, Northwest Africa. Oceanologica Acta, special vol. 19, 61–70.

Hagen, E., Schemeinda, R., Michelchen, N., Postel, L., Schulz, S., 1981. Zur küstensenkrechten Struktur des Kaltwasserauftriebs vor der Küste Namibias. Geodätische und Geophysikalische Veröffentlichungen, R. IV H. 36, 99pp.

Hart, T.J., Currie, R.I., 1960. The Benguela Current. Discovery Reports 31, 123–298.

Lass, H.U., Schmidt, M., Mohrholz, V., Nausch, G., 2000. Hydrographic and current measurements in the Angola-Benguela front area. Journal of Physical Oceanography 30, 2589–2609.

Lass, H.U., Prandke, H., Liljebladh, B., 2003. Dissipation in the Baltic Proper during Winter Stratification. Journal of Geophysical Research 108 (C6), 3187.

LeBlond, P.H., Mysak, L.A., 1978. Waves in the Ocean. Elsevier, Amsterdam, Oxford, New York 602pp.

Mooers, Chr.N.K., 1973. A technique for the cross spectrum analysis of pairs of complex-valued time series, with emphasis on properties of polarized components and rotational invariants. Deep-Sea Research 20, 1129–1141.

Mohrholz, V., Schmidt, M., Lutjeharms, J.R.E., 2001. The hydrography and dynamics of the Angola-Benguela frontal zone and environment in April 1999. South African Journal of Science 97, 199–208.

Nelson, G., 1989. Poleward motion in the Benguela area. In: Neshyba, S.J., Mooers, Ch.N.K., Smith, R.L., Barber, R.T. (Eds.), Poleward Flows Along Ocean Boundaries. Coastal and Estuarine Studies, vol. 34. Springer, New York, pp. 110–130.

Nelson, G., Hutchings, L., 1983. The Benguela upweling area. Progress in Oceanography 12, 333–356 (Pergamon).

Pawlowicz, R., Beardsley, B., Lentz, S., 2002. Classical Tidal Harmonic Analysis Including Error Estimates in MATLAB using T_TIDE. Computers and Geosciences 28, 929–937.

Poole, R., Tomczak, M., 1999. Optimum multiparameter analysis of the water mass structure in the Atlantic Ocean thermocline. Deep-Sea Research 46, 1895–1921.

Simpson, J.H., Hyder, P., Rippeth, T.P., Lucas, I.M., 2002. Forced oscillations near the critical latitude for diurnal-inertial resonance. Journal of Physical Oceanography 32, 177–187.

Shannon, L.V., 1985. The Benguela Ecosystem: evolution o fthe Benguela, physical features and processes. Oceanography and Marine Biology 23, 105–182.

Shannon, L.V., Nelson, G., 1996. The Benguela: large scale features and processes and system variability. In: Wefer, G., Berger, W.H., Siedler, G., Webb, D.J. (Eds.), The South Atlantic: Past and Present Circulation. Springer, Berlin, Heidelberg, pp. 163–210.

Stander, G.H., 1964. The Benguela Current off South West Africa. Investl. Rep. Mar. Res. Lab. S. W. Afr. 12 43pp., plus Plates 5-81.

Weeks, S.J., Currie, B., Bakun, A., Peard, K.R., 2004. Hydrogen sulphide eruptions in the Atlantic Ocean off southern Affrica: implications of a new view based on SeaWiFS satellity imagery. Deep-Sea Research I 51, 153–172.

Whiteman, C.D., Bian, X., 1995. Radar wind profiler observations of solar semidiurnal tides. Geophysical Research Letters 22 (8), 901–904.

Yamagata, T., Iizuka, S., 1995. Simulation of the subtropical domes in the Atlantic: a seasonal cycle. Journal of Physical Oceanography 25, 2129–2140.